IMPACT OF FISH SCALE-INSPIRED BIONIC BLADES ON THE AERODYNAMIC PERFORMANCE OF LARGE WIND TURBINES

Yuanjun DAI [1,2*], Wenjun ZHAO [1], Baohua LI [1]

This study proposes a fish-scale bionic blade to enhance the aerodynamic performance of large wind turbine blades. Twenty-one combinatorial schemes were designed based on the geometric characteristics of fish scales and computationally simulated using computational fluid dynamics (CFD) software. The results demonstrate that the circular fish scale bionic blade has superior aerodynamic performance across all operating conditions. Furthermore, the blades under the (P-rs5) scheme exhibit superior aerodynamic performance across various operating circumstances. In comparison to the prototype blade, the lift enhancement is 2.42% under rated conditions and 3.19% under non-rated conditions.

Keywords: Large wind turbine; Fish-scale bionic blade; Aerodynamic performance

1. Introduction

Due to the exhaustion of fossil fuels and heightened pollution, experts worldwide are exploring wind energy as a clean and sustainable alternative. Future forecasts suggest that wind energy will ultimately supplant conventional fossil fuel sources[1, 2]. Wind energy possesses several advantages compared to alternative energy sources, including its sustainability, absence of pollution, and extensive distribution [3]. Currently, the equipment employed for harvesting wind energy is wind turbines. Wind turbines can be classified as horizontal-axis or vertical-axis wind turbines based on the orientation of their blade rotation axis relative to the wind direction[4, 5]. Blades are essential for enhancing the efficiency of wind energy harnessing in wind turbines. Consequently, improving the aerodynamic efficiency of wind turbine blades has emerged as a significant global concern.

The application of bionics has emerged as a significant study way in the domain of wind turbine aerodynamic performance investigation. Experts and

[1]School of Mechanical Engineering, Shanghai Dianji University, China, e-mail: daiyj@sdju.edu.cn. (corresponding author)
[2]School of Aeronautical Mechanical and Electrical Engineering, Chongqing Aerospace Polytechnic, China, e-mail: daiyj@sdju.edu.cn.

researchers in relevant disciplines have conducted several studies on enhancing the aerodynamic efficiency of wind turbine blades, primarily categorized into the following two elements.

In bionic airfoil research, Dai Y J et al. [6] designed a novel wind turbine blade airfoil featuring an aerodynamic design inspired by an eagle. Computational fluid dynamics (CFD) analyses indicated that the bionic airfoil configuration enhanced the aerodynamic characteristics of the blade relative to the NACA2412 airfoil design. Huang S X et al. [7] developed dolphin-inspired airfoils for horizontal-axis wind turbines. The Dol-Rot 24°-2 airfoil significantly improved lift coefficients, while the Dol-Rot 24° design effectively suppressed flow separation on the suction surface compared to conventional S809 airfoils.

In optimizing blade design, Uzun et al.[8]drew inspiration from natural organisms to enhance aerodynamic performance by incorporating winglets and annular airfoils at the blade wing tips. The findings indicated that, in certain instances, the incorporation of an annular airfoil structure could enhance the aerodynamic efficiency of the blade by 6%. A study conducted by M. Manolesos et al. [9]investigated the potential of implementing vortex generators (VGs) on tidal turbine blades to enhance performance. Through computational fluid dynamics (CFD) simulations, the study demonstrated that low-profile VGs are helpful in minimizing flow separation and boosting blade performance. This illustrates the prospective utility of VGs in the design of tidal turbine blades. Zhang et al. [10] examined the aerodynamic properties of bionic blades located on the leading edge of the pectoral fin of the humpback whale. The model was developed using image processing technology and analyzed by CFD, revealing that the lift coefficient and lift-to-drag ratio of the bionic blade surpass those of the conventional model, indicating significant engineering value. He Z Y et al. [11] examined the influence of vortex generator parameters on the aerodynamic properties of wind turbine blades, optimizing the shape and position of the vortex generator via numerical simulation. It was discovered that the aerodynamic performance and power generation efficiency of the blades can be markedly enhanced under certain conditions.

The above scholars have conducted in-depth research on the bionic optimization design of wind turbine blades. Although the current study has made progress in airfoil optimization and small wind turbine blade design, the direction of bionic design for large wind turbine blades still needs to be further explored. This study observes the role of fish-scale dams in nature and considers the application of fish-scale structures to wind turbine blades, which is essential for improving the efficiency of wind energy utilization in large turbines and promoting technological innovation. In recent years, biomimetic assimilation has provided innovative paths for solving practical problems by systematically mapping similarity criteria between biological prototypes and engineering

designs[12]. In bionic assimilation research, the function-oriented school advocates performance enhancement by extracting the core hydrodynamic principles of biological prototypes, allowing for abstract simplification of form[13]; The Morphological Fidelity School emphasized the exact reproduction of geometric features[14]; System Synergist proposes a cross-scale dynamic similarity criterion[15]. In this study, morphological similarity criteria were used: based on macroscopic geometrical features of crucian, *Salmo salar*, and *Seriola dumerili*, such as circular cycloid, circular and triangular contours. Their dimensional parameters (height, width, radius, etc.) were also extracted and structural reproduction was achieved by 3D modeling. The bionic model and the biological prototype exhibit congruence in key geometric dimensions.

This study looks at a large 8MW horizontal axis wind turbine and designs multiple sets of bionic fish scale parallel arrangement blades to evaluate their impact on aerodynamic performance. The paper is organized as follows: Section 2 describes the design modeling of the bionic fish scale blade and the numerical simulation setup. Section 3 evaluates the effect of the bionic fish scale blade on the aerodynamic performance of the wind turbine. Section 4 provides a summary of the study.

2. Geometry model and simulation setup

2.1 Blade Geometric Parameters

The choice of airfoil type is crucial for wind turbine efficiency; it should aim to optimize the lift-to-drag ratio to enhance performance, while the root section should utilize an airfoil with greater relative thickness to ensure the structural integrity of the large blade. This study presents a design for a large wind turbine blade utilizing a multi-airfoil configuration, with the specific airfoil and angle distribution derived by Q-Blade and MATLAB software processing displayed in Table 1. The geometric specifications of the 8MW wind turbine blade are shown in Table 2, where the section positions are divided relative to the blade root. For the table the wind energy utilization factor is defined as follows:

$$C_p = \frac{P}{0.5\rho A V^3} \tag{1}$$

P is the output power of the wind turbine, A is the swept area of the wind turbine, V is the incoming wind speed, and ρ is the air density.

Table 1

Parameters of the blade airfoil

Proportionality coefficient	Section position [m]	Chord length [m]	Torsion angle [°]	Incoming flow angle [°]	Angle of attack [°]	Airfoil
0.2	22	16.22	6.52	17.52	11.00	DU40
0.25	27.5	13.69	3.42	14.42	11.00	DU40
0.3	33	11.15	3.22	12.22	9.00	DU35
0.35	38.5	9.74	1.58	10.58	9.00	DU35
0.4	44	7.45	0.82	9.32	8.50	DU30
0.45	49.5	6.68	-0.18	8.32	8.50	DU30
0.5	55	5.40	-0.48	7.52	8.00	FFA-W3-241
0.55	60.5	4.93	-1.15	6.85	8.00	FFA-W3-241
0.6	66	4.54	-1.72	6.28	8.00	FFA-W3-241
0.65	71.5	2.83	-4.70	5.80	10.50	DU21
0.7	77	2.63	-5.11	5.39	10.50	DU21
0.75	82.5	2.44	-0.98	5.02	6.00	NACA4418
0.8	88	2.29	-1.31	4.69	6.00	NACA4418
0.85	93.5	2.16	-1.61	4.39	6.00	NACA4418
0.9	99	2.04	-1.92	4.08	6.00	NACA4418
0.95	104.5	1.90	-2.26	3.74	6.00	NACA4418
1	110	1.53	-2.76	3.24	6.00	NACA4418

Table 2

Parameters and specifications of an 8MW wind turbine blade

Blade parameters	Parameter value
Blade number	3
Length of leaf blade [m]	110
Diameter of wind wheel [m]	228
Leaf tip velocity ratio	7
Wind energy utilization factor	0.41
Rated power of wind turbine [MW]	8
Rated speed rad [min]	5.864
Rated wind speed [m/s]	10

2.2 Design of bionic fish scale blades

The diversity of fish in nature is exhibited in several forms, including the morphology of fish scales. Three representative fish species were chosen for this study: crucian, *Salmo salar*, and *Seriola dumerili*. Figure 1 illustrates that the scale morphology of crucian carp is fan-shaped (a type of circular cycloid scale); *Salmo salar* scales exhibit a characteristic circular morphology; and *Seriola dumerili* scales display a triangular shape in certain regions.

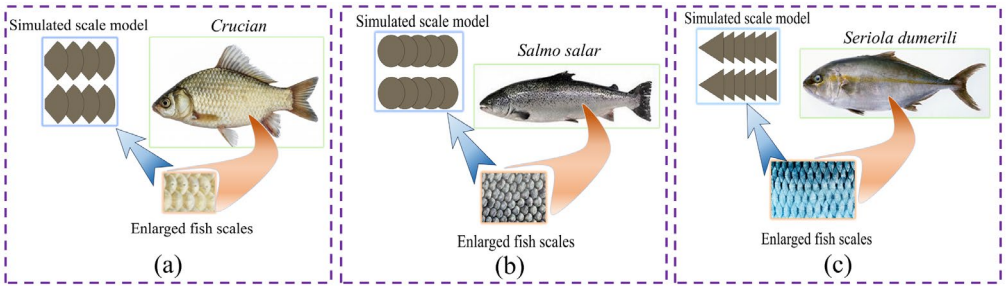

Fig. 1. Diverse Fish Scale Diagrams (a) Carp scales; (b) *Salmo salar* scales; (c) *Seriola dumerili* scales.

This investigation established the experimental structure of fish scales as described by Dey et al. [16], identifying the shapes as fan-shaped, round, and triangular scales. This study emphasized the macrostructure of the fish scales in the experiment and neglected the microscopic features. The primary research seeks to examine the impact of different fish scale arrangement schemes on the aerodynamic efficiency of wind turbines.

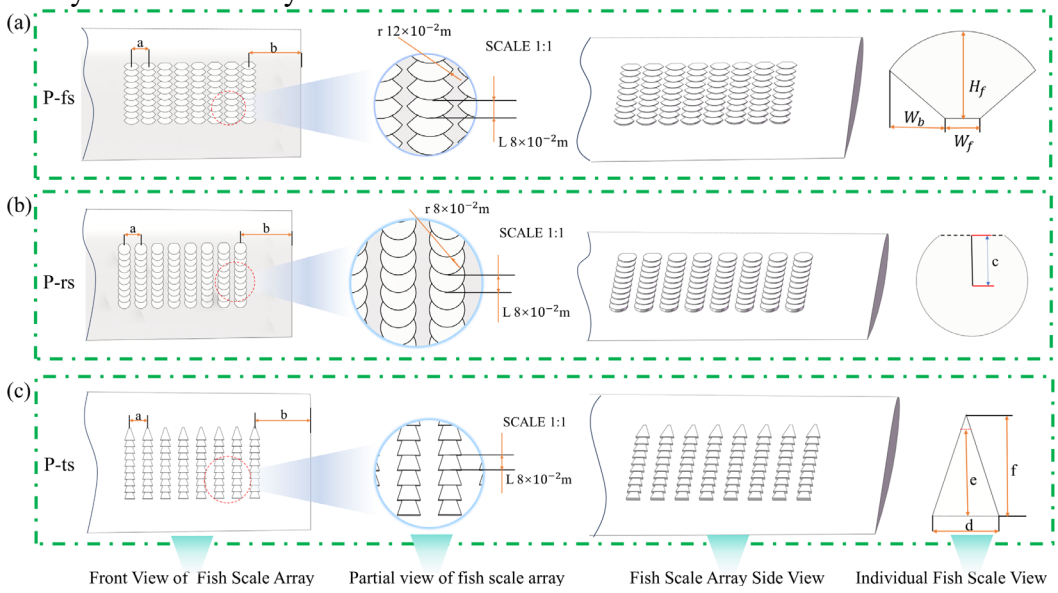

Fig. 2. Various views and sizes of fish scales on the blade (a) Scalloped Fish Scale View and Dimensions (b) Round Fish Scale View and Dimensions (c) Triangle Fish Scale View and Dimensions

Figure 2 depicts the distribution and dimensional maps of several fish scale blades. As can be seen from the frontal view of the fish scale array in Fig. 2, the fish scale model in this study was laid on the upper surface of the blade on one side located at the tip of the blade (the fish scale structure in the upper right corner is located at 21% of the blade tip chord length at a lateral distance of "b"), showing a parallel arrangement. The lateral spacing "a" of the fish scales is

variable, and the distance “b” of the rightmost fish scale from 21% of the chord length of the leaf tip was 0.7 m. The quantity of transverse fish scale arrays is 8, whereas the number of fish longitudinal scale arrays is 10. The longitudinal spacing “L” of the fish scales, as depicted in the partial view of the fish scale array in Fig. 2, measures $8 \times 10^{\wedge-2}$ m. The thickness of all three shapes of fish scale structures in the initial row is set to $3 \times 10^{\wedge-2}$ m. After arraying on the curved surface, the upper surface of the rear row is about $1\times 10^{\wedge-2}$ m higher than that of the neighboring front row, which ensures the consistency of the arrangement regularity.

The dimensional parameters of the individual sector scales in Fig. 2(a) are as follows: the height of the scale H_f is 12×10^{-2} m, the width of the scale front edge W_f is 4.8×10^{-2} m, the width of the scale side edge W_b is 8×10^{-2} m, and the radius of the upper circle of the scale “r” is 12×10^{-2} m. The radius of the circular fish scale depicted in Fig. 2(b) is 8×10^{-2} m. A portion of the circular fish scale is embedded inside the blade, and the distance “c” from the center of the junction of the exposed portion to the center point of the circle is 5×10^{-2} m. In the dimensional parameters of the individual triangular scales in Fig. 2(c), the scale height “f” is 19×10^{-2} m, the exposed height e of the scale is 16×10^{-2} m, and the scale width “d” is 12×10^{-2} m.

Table 3 consists of any combination of fish scale shapes, lateral spacing, and parallel arrangement to form 21 fish scale arrangement schemes.

Table 3

Combined scheme of fish scale bionic blade structure

Horizontal spacing(m)	Arrangement scheme for fish scale blades						
	0.19	0.21	0.22	0.24	0.25	0.26	0.28
Parallel rows of fan-shaped fish scales	P-fs1	P-fs2	P-fs3	P-fs4	P-fs5	P-fs6	P-fs7
Parallel rows of round fish scales	P-rs1	P-rs2	P-rs3	P-rs4	P-rs5	P-rs6	P-rs7
Parallel rows of triangular fish scales	P-ts1	P-ts2	P-ts3	P-ts4	P-ts5	P-ts6	P-ts7

2.3 Numerical simulation

This study utilized the commercial computational fluid dynamics (CFD) software program Fluent (2023R2) for simulations. In this study, the fluid is considered incompressible. In dealing with the problem of turbulent stresses present in a nonconstant turbulence model, the Navier-Stokes equations are combined with Reynolds averaging, and the turbulent stresses are represented by the following equations:

$$\frac{\partial(\rho u_i)}{\partial x_i} = 0 \tag{2}$$

$$\frac{\partial(\rho u_i)}{\partial t} + \frac{\partial(\rho u_j u_i)}{\partial x_j} = -\frac{\partial p}{\partial x_i} + \frac{\partial}{\partial x_j}\left[\mu\left(\frac{\partial u_i}{\partial x_j} + \frac{\partial u_j}{\partial x_i} - \frac{2}{3}\delta_{ij}\frac{\partial u_i}{\partial x_j}\right)\right] + \frac{\partial}{\partial x_i}\left(-\rho\overline{u_i' u_j'}\right) \tag{3}$$

x_i and u_i represent the position and relative velocity of the fluid in the Cartesian coordinate system, while p and ρ denote the pressure and fluid density in the flow field, δ_{ij} denotes the Kronecker function, and μ indicates the dynamic viscosity of the fluid. In order to close the URANS equation, the $k-\omega$ (SST) shear stress model is used [17]. The SST $k-\omega$ shear stress model is a prevalent method for studying and determining the aerodynamic characteristics of wind turbines [18].

2.3.1 Aerodynamic coefficients

This section enumerates the formulas employed to compute aerodynamic coefficients, including lift and drag[19, 20]. These aerodynamic coefficients remain significant in various ways for quantifying the underlying flow field information. Employing the coefficient form leverages the benefit of dimensionless parameters, facilitating the reproducibility of results due to their dimensional independence. The lift F_L and the drag F_D [21] are expressed as equations (4) and (5) provided below :

$$F_L = \frac{C_l \rho V^2 S}{2} \tag{4}$$

$$F_D = \frac{C_d \rho V^2 S}{2} \tag{5}$$

Where F_L and F_D denote lift and drag, C_l and C_d represent the lift and drag coefficients of the airfoil, S indicates the reference area, V signifies the wind speed, and ρ refers to the air density.

2.3.2 Computational domain and boundary conditions

In this research, the simulation methodology used in the literature [22] is adopted, taking into account the flow and rotational symmetry of the wind turbine in order to optimize the computational efficiency and focusing only on the wind turbine blades in the simulation, excluding other components such as hubs and towers. The face of the rotational domain in contact with the outer domain is set up as an interface, which allows data exchange between the two regions. The flow field outside the computational domain is one-third cylindrical with a length of 6D

(D is the diameter of the wind turbine) and a circular radius of 1.5D, and periodic boundary conditions are set at the sides. The spinning zone is positioned 1D from the entrance and 5D from the exit, with a radius of 125m and a thickness of 40m. And the blade root is 4 meters away from the rotation axis. Figure 3 illustrates the introduction of wind speed via the velocity intake, traversing the computational domain, and exiting through the pressure outlet.

The velocity inlet at the entrance, the pressure outlet at the exit, and additional components constitute the boundary conditions. The turbulence intensity is 1%, and the relative pressure at the outlet is 0 Pa[23]. This study employs two operational circumstances to replicate the actual functioning environment of the wind turbine more precisely. The rated wind speed is 10m/s, and the rotational speed is 5.864rad/min. The non-rated wind speed is 8 m/s, and the rotational speed is 4.351 rad/min.

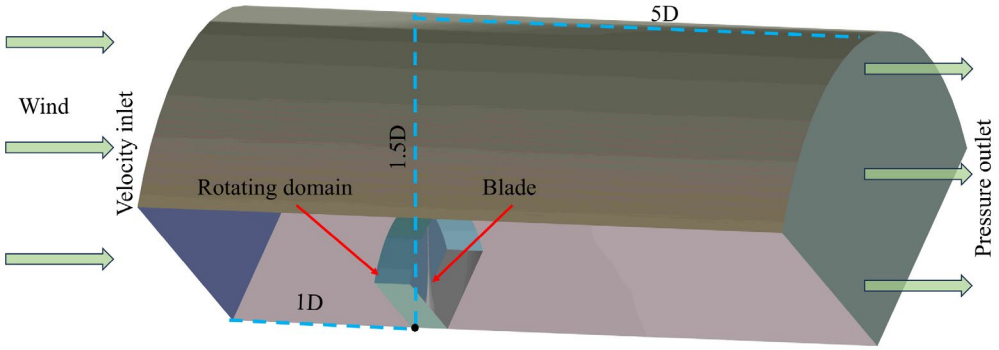

Fig. 3. Schematic diagram of boundary conditions and computational domain

2.3.3 Meshing and solvers

The computational and rotational domains are organized via unstructured meshing in Fluent Meshing. Figure 4(a) depicts the comprehensive and localized meshing, and Figure 4(b) presents a schematic representation of the meshing of the three fish scales. Generation of prismatic boundary layers on wind turbine blade faces: the prismatic layer consisted of 10 layers, each with an elongation of 1.12 to keep the Y+ value within 1. The height of the first grid layer was 3.4×10^-4m. The SIMPLE iterative algorithm is employed for numerical simulation of the flow field, with the convergence of the residuals determined when their values stabilize, the difference between inlet and outlet flow rates is below 10%, and the residuals are consistently reduced to 10^-4.

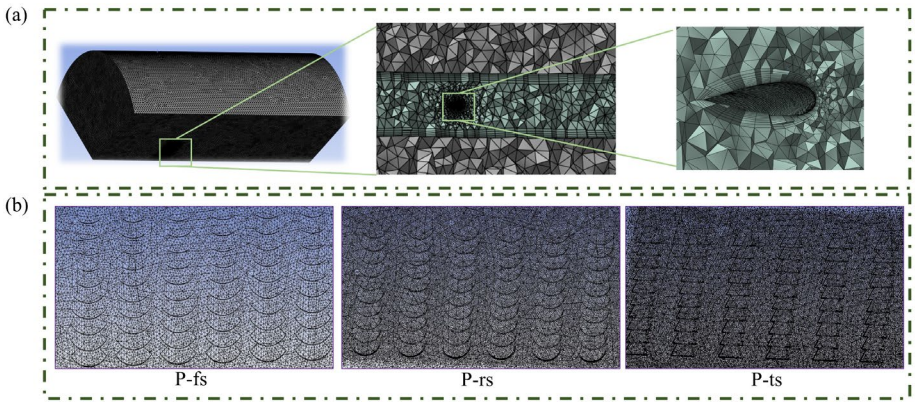

Fig. 4. Grid View (a) Global and local grid views (b) Three fish scale grid views

2.3.4 Grid-independent verification

Modifying the fundamental mesh size in Fluent meshing consistently produces three categories of meshes: coarse, medium, and refined. The lowest orthogonal mass for all three meshes exceeds 0.1, signifying superior mesh quality.7569075, 10221075, and 13322100 correspond to coarse, medium, and fine grids. Table 4 gives the power coefficient values of the P-fs1 wind turbine blades at three different meshes for non-rated operating conditions. The disparity in the power coefficients between the fine and medium grids is about 0.9%. The discrepancy between coarse and medium grids is 9.1%. Consequently, this study used a medium grid as a benchmark to reduce computational burden and guarantee the precision of the results. For different fish scale geometric features of the blade, encryption is carried out in the local area, and the overall mesh density is similar to that of the benchmark. Furthermore, parameters such mesh orthogonality quality are assessed for all schemes, and they all fall inside the acceptable range, meeting the computational criteria. Table 5 lists the specifications of the servers used in this study.

Table 4

Power coefficients of P-fs1 blades in three grids

Mesh Type	Coarse grid	Medium grid	Fine grid
Number of grids	7569075	10221075	13322100
Power coefficients	0.0655	0.0721	0.0728

Table 5

Server specifications

Computer core component	Name and Size
CPU	Intel (R) Xeon (R) Platinum 8272CL CPU @2.60GHz
Kernel	52
Operating system	Window 10
Disk	NS300 256G SSD、Lenovo SSD ST510 120G、Hitachi HUA723030ALA641
Logic processors	104
RAM	192GB

3. Analysis and discussion of numerical results

In this section, numerical simulation experiments are conducted to investigate the effect of various fish scale arrangement schemes on the aerodynamic performance of wind turbine blades under different operating conditions. The aerodynamic performance parameters are also compared with those of the prototype blade (Pb).

3.1 Analysis of output torque of various fish scale bionic blades

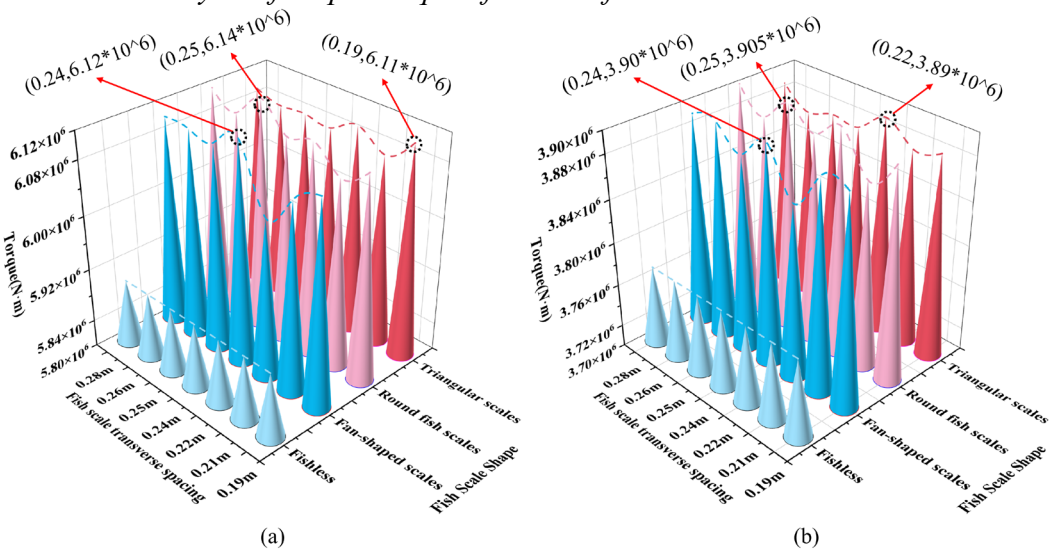

Fig. 5. Output torque diagram of each fish scale bionic blade under different working conditions (a) Output torque diagram at rated operating conditions (b) Output torque diagram under non-rated operating conditions

Figure 5 illustrates the output moments of the fish scale bionic blades under different operational conditions. The figure shows that different fish scale arrangement schemes have a significant effect on the output torque of the blades. Numerical simulations show that at higher-rated operating wind speeds, the higher the output torque of the blades means the higher the output power, which is in line with the findings of the literature [24].

Figure 5 illustrates that the torque value of each fish scale-inspired blade surpasses that of the prototype blade (Pb). Figure 5(a) depicts the output moment of the blade under rated conditions. In comparison to the prototype blade, the fan-shaped fish scale blade exhibits a 3.87% enhancement at a lateral pitch of 0.24 m, the circular fish scale blade shows a 4.08% improvement at a lateral pitch of 0.25 m, and the triangular fish scale blade demonstrates a 3.65% increase at a lateral pitch of 0.19 m. Figure 5(b) illustrates the blade output torque under non-rated conditions. In comparison to the prototype blade output torque values, the fan-shaped fish scale blades exhibited a 3.36% enhancement at a lateral

spacing of 0.24 m, the circular fish-scale blades demonstrated a 3.52% improvement at a lateral spacing of 0.25 m, and the triangular fish-scale blades recorded a 3.27% increase at a lateral spacing of 0.22 m.

Further analysis of the figure indicates that the blades in the scheme (P-rs5) exhibit superior aerodynamic performance across various operating circumstances. The torque enhancement rate is greatest for the circular fish-scale blade, followed by the sectoral fish-scale blade, and lastly, the triangle fish-scale blade. The torque enhancement rate of triangular fish-scale blades is very modest and generally steady.

3.2 Analysis of power coefficient plots of various fish scale bionic blades

The preceding section studied the blade's output torque, followed by an examination of the blade's power coefficient, as illustrated in Fig. 6. The power coefficient is a parameter essential for calculating the productivity of a wind turbine or wind farm[25]. This is defined as presented in Equation 6.

$$C_{p,\text{blade}} = \frac{P_{\text{blade}}}{0.5\rho A V^3} \tag{6}$$

Where P_{blade} is the blade output power, and A is the swept area of the wind turbine.

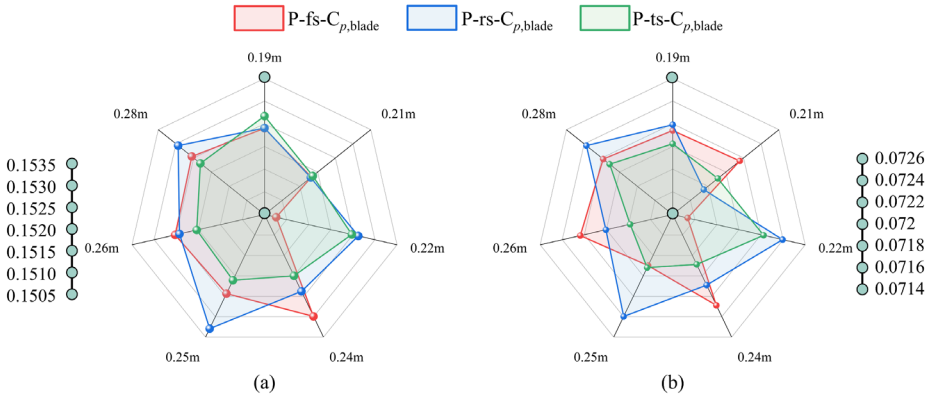

Fig. 6. Directional plot of blade power coefficient (a) Orientation diagram of power coefficients at rated conditions (b) Directional plot of power coefficients for non-rated conditions

Figure 6(a) illustrates the power coefficient distribution of the fish-scale bionic blades at rated operating conditions. The power coefficient of the scalloped fish scale blade is minimized at a lateral spacing of 0.22 m and maximized at 0.24 m. The power coefficient of the circular fish scale blade is lowest at a lateral spacing of 0.21m, reaches a maximum of 0.25m, and then decreases progressively. The power coefficient of the triangular fish scale blade was lowest at a lateral spacing of 0.21m, then increasing to a maximum of 0.19m. Figure 6(b) illustrates the power coefficient graphs of the blades under non-rated operating conditions.

The power coefficient graphs for fan-shaped fish scale blades and circular fish scale blades resemble those under rated operating conditions and demonstrate good aerodynamic performance across various transverse pitches. The power coefficient of the triangular fish-scale blade reaches its greatest at a lateral length of 0.22 m and its minimum at a lateral length of 0.26 m.

All three configurations of fish-scale bionic blades exhibit superior aerodynamic performance at a lateral fish-scale spacing of 0.22 to 0.25 meters. In comparison to the other two fish scale shapes, the circular fish scale blade has superior aerodynamic performance and holds greater significance for engineering applications.

3.3 Analysis of aerodynamic performance parameters of various fish scale bionic blades

3.3.1 Analysis of lift and drag parameter values

Lift and drag are critical assessment metrics in aerodynamic research and industrial applications[26] because they have a significant impact on energy performance and determine further applications.

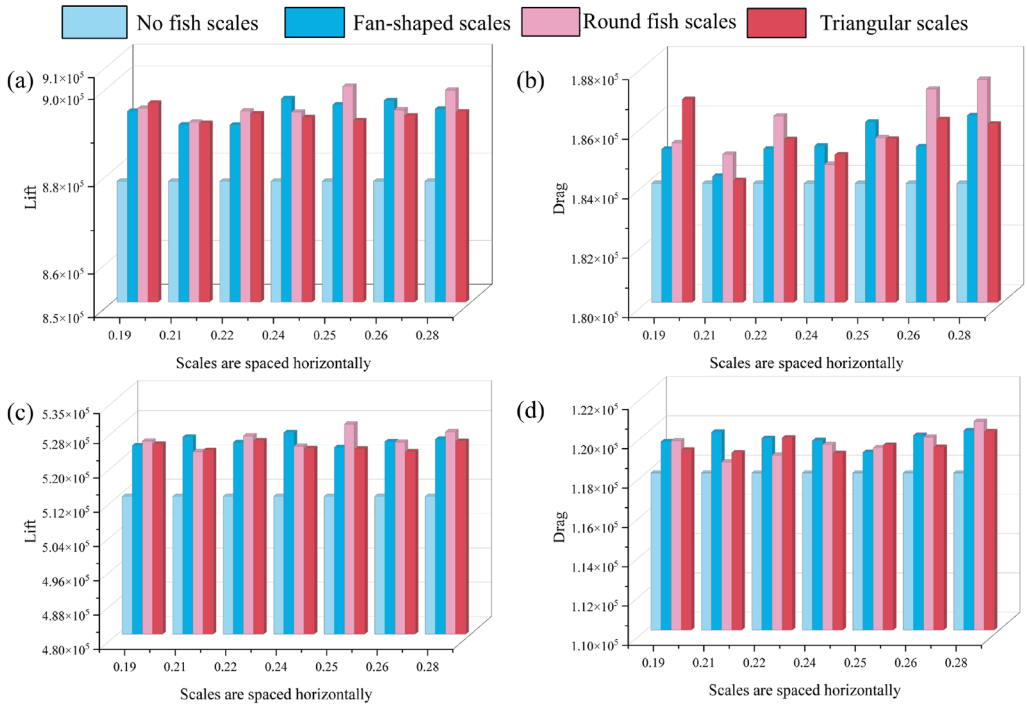

Fig. 7. Aerodynamic parameters under different operating conditions (a) Lift values at rated operating conditions (b) Drag value at rated operating conditions (c) Lift values for non-rated operating conditions (d) Drag value at non-rated operating conditions

This study demonstrates that incorporating fish scales at the blade tip increases surface roughness, hence increasing the fluid's frictional resistance

against the blade surface[27]. Figures 7(b) and 7(d) illustrate that the frictional resistance faced by the fluid flow over the fish-scale blade's surface escalates, resulting in heightened wind resistance. Simultaneously, the lift of the fish scale bionic blades has been substantially increased.

Figure 7 illustrates the lift and drag characteristics of the fish scale bionic blade under various operating conditions. Figure 7(a) demonstrates that the lift of parallel distributed fan-shaped fish scales at rated settings shows improvements of 1.80%, 1.46%, 1.45%, 2.11%, 1.96%, 2.06%, and 1.86%, respectively, relative to the blades without fish scales. The lift of the circular fish scale was improved by 1.87%, 1.52%, 1.80%, 1.78%, 2.42%, 1.83%, and 2.33%, respectively, compared to the blade devoid of fish scales. The lift of triangular fish scales improved by 2.00%, 1.49%, 1.73%, 1.64%, 1.56%, 1.68%, and 1.78%, respectively, compared to the non-fish scale blades. Fan-shaped fish-scale blades provide superior aerodynamic performance at a lateral spacing of 0.24 meters (P-fs4). Round fish scale blades exhibit superior aerodynamic performance with a lateral fish scale spacing of 0.25 m (P-rs5). The triangular fish-scale blades exhibit superior aerodynamic performance at a lateral fish-scale spacing of 0.19 m (P-ts1).

Figure 7(c) illustrates the lift comparison under non-rated operating conditions. The scalloped fish-scale blade demonstrates enhanced aerodynamic efficiency at a transverse fish-scale pitch of 0.24 m (P-fs4), yielding a lift augmentation of 2.83% relative to the non-fish-scale blade. The rounded fish-scale blades demonstrate enhanced aerodynamic efficiency at a transverse fish-scale spacing of 0.25 meters (P-rs5), resulting in a lift augmentation of 3.19%. The triangular fish-scale blades exhibited superior aerodynamic performance at a lateral scale spacing of 0.22 m (P-ts3), resulting in a lift enhancement of 2.48%.

The above analysis demonstrates that the fish-scale bionic blade under the (P-rs5) scheme exhibits substantial lift enhancement across various operating situations, thereby substantiating the enhancement of energy performance, engineering significance, and application value.

3.3.2 Lift resistance ratio parameter value analysis

Figure 8 illustrates the blade lift-to-drag ratio characteristics for the two fish-scale configurations under the two operational situations. The lift-to-drag ratio of the blade sans fish scale is 4.77 under rated conditions and 4.34 under non-rated conditions. Figure 8(a) illustrates that the lift-to-drag ratio of the fan-shaped fish-scale blade with a fish-scale spacing of 0.24 m (P-fs4) at rated operating conditions is 4.84, representing an increase of 1.47% compared to the no-fish-scale blade. The lift-to-drag ratio for round fish scale blades with a fish scale spacing of 0.25 m (P-rs5) is 4.848, representing an increase of 1.64% compared to blades without fish scales. At a fish scale spacing of 0.21 m (P-ts2), the lift resistance ratio of triangular fish scale blades was 4.839, representing a

1.45% increase compared to non-fish scale blades.

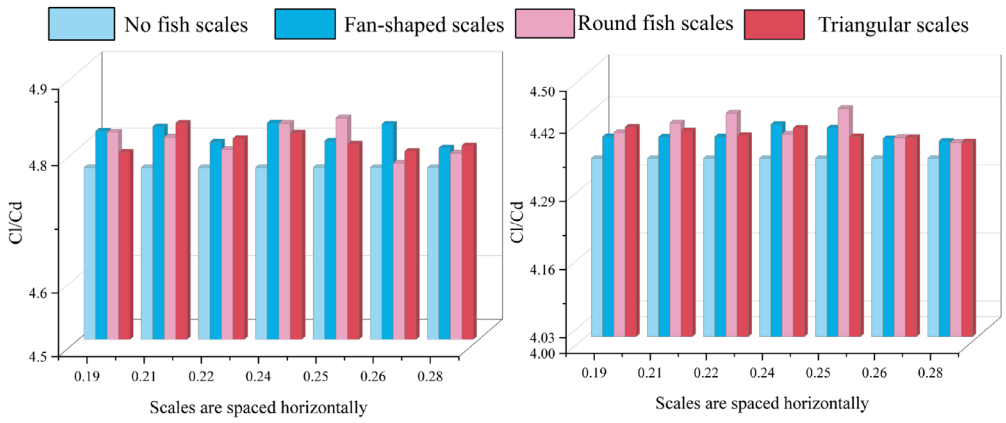

Fig. 8. Analysis of Lift-to-Resistance Ratio of Fish Scale Blade (a) Blade parameter diagram at rated operating conditions (b) Blade parameter plot for non-rated operating conditions

In the non-rated operation depicted in Fig. 8(b), the lift-to-drag ratio of the fan-shaped fish-scale blades is 4.405 at a fish-scale spacing of 0.24 m (P-fs4), representing a 1.5% increase compared to the non-fish-scale blades. The lift-to-drag ratio of round fish scale blades is 4.44 at 0.25 m (P-rs5), representing a 2.3% increase compared to blades without fish scales. The lift-resistance ratio of triangular fish scale blades was 4.39 at a fish scale spacing of 0.19 m (P-ts1), representing a 1.15% increase compared to non-fish scale blades.

Overall, both (P-fs4) and (P-rs5) exhibit superior lift-to-drag ratio characteristics throughout varying operating conditions. (P-rs5) scheme with better blade lift-to-drag ratio characteristics.

3.4 Relative Pressure Distribution Cloud

3.4.1 Analysis of Blade Section Relative Pressure Maps

As shown in Fig. 9, this subsection presents a cloud of blade slices of a fish scale bionic blade at rated operating conditions to visually assess the effect of the fish scale on the aerodynamic performance of the blade.

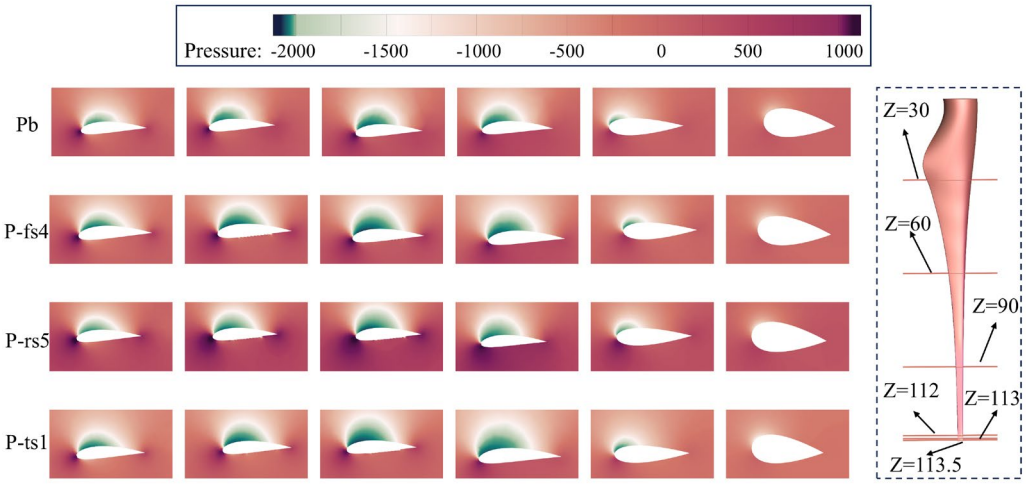

(a)Z=113.5 (b)Z=113 (c)Z=112 (d)Z=90 (e)Z=60 (f)Z=30 (g)

Fig. 9. Fish scale bionic blade relative pressure slicing cloud map

This study selected three cross-sections at the blade tip in the unfolding direction: Z=113.5, Z=113, and Z=112; one cross-section at a distance from the blade tip, Z=90. A cross-section was selected in the middle of the blade and named Z=60, and one cross-section near the blade root, Z=30. To illustrate the cross-sectional distribution, the entire blade was sliced and partitioned, as depicted in Fig. 9(g). The relative pressure differential near the blade's tip is maximal, and the impact of this variation is obvious, as illustrated in the aforementioned image, supporting the findings in the literature [28].

The relative pressure clouds indicate that the varying distribution of pressure values on the blade's pressure and suction surfaces increases aerodynamic loads at the blade's leading edge and produces a maximum differential pressure at the tip area. The fish-scale bionic blade exhibits superior lift and other properties relative to the prototype blade, with the surface pressure differential of the blade being intricately linked to its energy performance[29]. Fig. 10 illustrates a cloud representation of the pressure distribution at the tip section of the prototype blade. Table 6 presents the maximum blade pressure values at the tangential plane (Z=112) for various configurations, utilizing the thermal probe function of the post-processing program Tecplot. Table 6 indicates that the differential pressure values for all three fish-scale blades surpass those of the non-fish-scale blades, with the P-rs5 blades exhibiting greater differential pressure values than the P-fs4 blades and the P-fs4 blades demonstrating higher differential pressure values than the P-ts1 blades. This further suggests that the aerodynamic performance of the blade is greatly improved under the (P-rs5) scheme discussed in the previous sections.

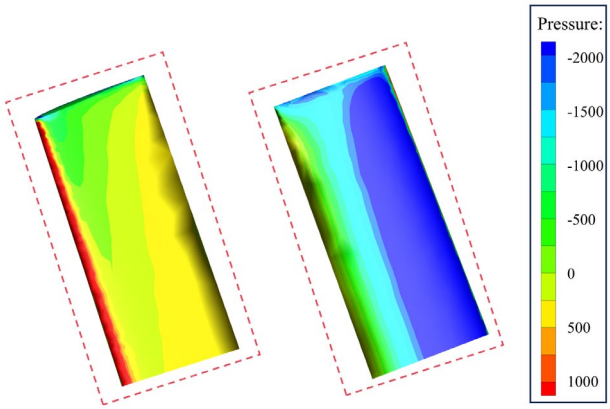

Fig. 10. Blade pressure cloud (a) Pressure surface (b) Suction surface

Table 6

Maximum blade pressure at slice Z=112

Fish Scale Scheme	Positive pressure/(Pa)	Negative pressure/(Pa)	Differential Pressure of the Blade/(Pa)
Pb	2154.47	-3508.72	5663.19
P-fs4	2221.6	-3600	5821.6
P-rs5	2308	-3682	5990
P-ts1	2165	-3580	5745

3.4.2 Analysis of surface pressure maps in the leaf tip region

This section displays the surface pressure plots in the blade tip region at rated operating conditions, based on the study from previous sections, for the three aerodynamically superior schemes depicted in Fig. 11.

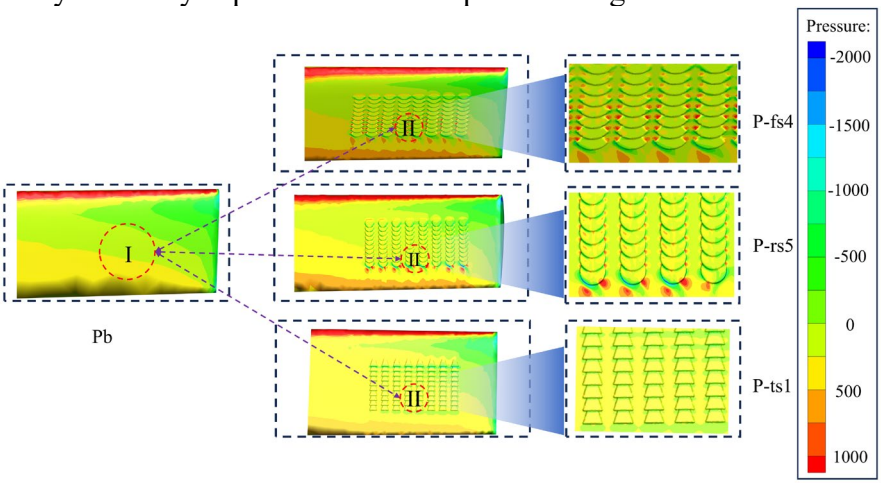

Fig. 11. Analysis of pressure exerted on fish scale surfaces

Figure 11 illustrates that the fish-scale structure increases the pressure on the blade surface in comparison to a smooth blade surface. In the (P-rs5) scheme, the pressure in the blade II region surpasses the surface pressure in the blade I region, and the extent of the high-pressure area progressively increases. The overall pressure difference in the tip region of the blade in this scheme is greater than that of the other two fish scale blades, which is more conducive to improving the aerodynamic energy of the blade, further validating the previous conclusions.

4. Conclusion

This work involved the bionic design and simulation of an 8 MW wind turbine blade. Twenty-one configurations of fish scales were designed by altering their shape and lateral spacing. The aerodynamic performance of the fish-scale blades is assessed by numerical simulations of several fish-scale arrangement configurations, leading to the following conclusions:

1) The bionic fish scale blade exhibits enhanced aerodynamic performance relative to the traditional blade. The numerical simulation analysis of the three fish scale blade configurations reveals that the circular fish scale blade demonstrates enhanced aerodynamic performance compared to the other two shapes. Under rated conditions, the output moments of circular fish scale blades (P-rs) in a parallel configuration are improved by 1.87%, 1.52%, 1.80%, 1.78%, 2.42%, 1.83%, and 2.33%, respectively, relative to the standard blades (Pb). The output torque of parallel aligned circular fish scale blades (P-rs) was enhanced by 2.46%, 2.00%, 2.69%, 2.24%, 3.19%, 2.42%, and 2.86%, respectively, relative to the standard blades (Pb) under non-rated working conditions.

2) Under rated conditions, the fan-shaped fish scale blade has better aerodynamic performance when the fish scale arrangement scheme is (P-fs4), the round fish scale blade is (P-rs5), and the triangular fish scale blade is (P-ts1). Under non-rated conditions, fan-shaped fish scale blades have better aerodynamic performance when the fish scale arrangement scheme is (P-fs4), round fish scale blades have better aerodynamic performance when the fish scale arrangement scheme is (P-rs5), and triangular fish scale blades have better aerodynamic performance when the fish scale arrangement scheme is (P-ts3).

3) The aerodynamic performance of all three fish scale bionic blades is better when the lateral spacing of fish scales is 0.22-0.25 meters. The fish scale bionic blades under the (P-rs5) scheme have better performance in terms of output torque, lift, etc., under different operating conditions. It is further verified that there exists a certain relationship between the pressure difference and the lift and other parameters.

4) In this study, the aerodynamic performance analysis of the fish scale bionic blade is mainly carried out through numerical simulation, and the accuracy of the results for practical applications is improved through the validation of mesh independence, the setting of different working conditions, and the analysis of the universality of the bionic parameters. However, it should be pointed out that this study lacks certain experimental validation, and the subsequent study will be analyzed by 3D printing a scaled-down blade for wind tunnel experiments.

5) Given the installation and subsequent maintenance costs, the fish scale bionic structure in this study may be glued to the blade via 3D printing. This approach may effectively decrease the installation costs of the intricate construction while also reducing subsequent maintenance requirements.

Acknowledgments

The National Natural Science Foundation of China supports this research project, project under Grant. (No. 51966018 and 51466015). All employees and schools acknowledged and supported this research initiative. The writers also recognize the assistance of anonymous reviewers.

REFERENCES

[1] *Z. Zhang, L. Kuang, Z. Han, D. Zhou, Y. Zhao, Y. Bao, L. Duan, J. Tu, Y. Chen, M. Chen,* Comparative analysis of bent and basic winglets on performance improvement of horizontal axis wind turbines, Energy 281 (2023) 128252.

[2] *G. Chen, X.-F. Liang, X.-B. Li,* Modelling of wake dynamics and instabilities of a floating horizontal-axis wind turbine under surge motion, Energy 239 (2022) 122110.

[3] *K. Wang, D. Wu, T. Zhang, L. Yin, K. Wu, C. Zheng,* Spatial distribution and long-term trend of wind energy in the Northwest Pacific Ocean, Water-Energy Nexus 7 (2024) 135-142.

[4] *H.Y. Peng, H.J. Liu, J.H. Yang,* A review on the wake aerodynamics of H-rotor vertical axis wind turbines, Energy 232 (2021) 121003.

[5] *L.N. Azadani,* Vertical axis wind turbines in cluster configurations, Ocean Engineering 272 (2023) 113855.

[6] *Y. Dai, D. Wang, X. Liu, W. Wu,* Optimized design and aerodynamic performance analysis of wind turbine blades with sparrowhawk bionic airfoil, U.P.B. Sci. Bull., Series D, vol. 86, no. 1, 2024, pp. 221-236.

[7] *S. Huang, H. Qiu, Y. Wang,* Aerodynamic performance of horizontal axis wind turbine with application of dolphin head-shape and lever movement of skeleton bionic airfoils, Energy Conversion and Management 267 (2022) 115803.

[8] *Uzun M, Özdemir M, Yıldırım Ç V, Çoban S,* A novel biomimetic wing design and optimizing aerodynamic performance, Journal of Aviation, 2022, 6(1): 12-25.

[9] *M. Manolesos, L. Chng, N. Kaufmann, P. Ouro, D. Ntouras, G. Papadakis,* Using vortex generators for flow separation control on tidal turbine profiles and blades, Renewable Energy 205 (2023) 1025-1039.

[10] *Z.-h. Zhang, W.-w. Li,* Aerodynamic characteristics of bionic wing of leading-edge of humpback whale flipper, Engineering Mechanics, vol. 37(S), June 2020, pp. 376-379,386.

[11] *H. Zhengyang,* Numerical Simulation Investigation of The Effect of Vortex Generator Parameters on Aerodynamic Characteristics of Wind Turbine Blade, Master's Thesis, Chongqing University, 2016.

[12] *S. Pathak,* Biomimicry: (Innovation Inspired by Nature), International Journal of New Technology and Research 5 (2019).

[13] *F.E. Fish, G.V. Lauder,* Control surfaces of aquatic vertebrates: active and passive design and function, The Journal of experimental biology 220(23) (2017) 4351-4363.

[14] *K. Autumn, M. Sitti, Y.A. Liang, A.M. Peattie, W.R. Hansen, S. Sponberg, T.W. Kenny, R. Fearing, J.N. Israelachvili, R.J. Full,* Evidence for van der Waals adhesion in gecko setae, Proceedings of the National Academy of Sciences 99(19) (2002) 12252-12256.

[15] *J.F.V. Vincent, O.A. Bogatyreva, N.R. Bogatyrev, A. Bowyer, A.-K. Pahl,* Biomimetics: its practice and theory, Journal of The Royal Society Interface 3(9) (2006) 471-482.

[16] *P. Dey, G. Hedau, S.K. Saha,* Experimental and numerical investigations of fluid flow and heat transfer in a bioinspired surface enriched microchannel, International Journal of Thermal Sciences 135 (2019) 44-60.

[17] *Z. Zhang, L. Kuang, Y. Zhao, Z. Han, D. Zhou, J. Tu, M. Chen, X. Ji,* Numerical investigation of the aerodynamic and wake characteristics of a floating twin-rotor wind turbine under surge motion, Energy Conversion and Management 283 (2023) 116957.

[18] *Q. Zhang, M. Bashir, W. Miao, Q. Liu, C. Li, M. Yue, P. Wang,* Aerodynamic analysis of a novel pitch control strategy and parameter combination for vertical axis wind turbines, Renewable Energy 216 (2023) 119089.

[19] *T. Cebeci, M. Platzer, H. Chen, K.-C. Chang, J. Shao,* Analysis of Low-Speed Unsteady Airfoil Flows, Springer Berlin Heidelberg, 2005.

[20] *I.H. Abbott, A.E.V. Doenhoff,* Theory of wing sections: Including a summary of airfoil data, Dover Publications, 1959.

[21] *S. Gudmundsson,* Chapter 16-Aircraft Drag Analysis, General Aviation Aircraft Design: Applied Methods and Procedures, Butterworth-Heinemann, 2022, pp. 657-752.

[22] *Z. Zhang, X. Zhang, C. Xu,* Study of aerodynamic noise for large-scale wind turbine blade, Acta Energiae Solaris Sinica, 38(5), 2017, pp. 1346-1353.

[23] *Z. Shen, S. Gong, G. Xie, H. Lu, W. Guo,* Investigation of the effect of critical structural

parameters on the aerodynamic performance of the double darrieus vertical axis wind turbine, Energy 290 (2024) 130156.

[24] *L. Gumilar, M. Sholeh,* Impact of Blade Length on the Horizontal Wind Turbine Output Power and Torque, 2020 International Seminar on Application for Technology of Information and Communication (iSemantic), IEEE, 2020, pp. 238-242.

[25] *H. Hwangbo, A. Johnson, Y. Ding,* A production economics analysis for quantifying the efficiency of wind turbines, Wind Energy 20(9) (2017) 1501-1513.

[26] *N. Sinaga, D.Y. Dhande, B. Yunianto,* A numerical investigation of the effect of blade number on the performance of an INSEAN E779A marine propeller in a cavitating flow using computational fluid dynamics, Ocean Engineering 261 (2022) 112063.

[27] *F. Lalegani, M.R. Saffarian, A. Moradi, E. Tavousi,* Effects of different roughness elements on friction and pressure drop of laminar flow in microchannels, International Journal of Numerical Methods for Heat & Fluid Flow 28(7) (2018) 1664-1683.

[28] *Z. Zhiwei, HUDanmei, WUZhixiang, Z. Kaihua,* Numerical Analysis on the Aerodynamic Characteristics of a Wind Turbine with Different Winglets, Journal of Chinese Society of Power Engineering 39(06) (2019) 486-491.

[29] *J. Zhang, R. Zhang, Z. Huang,* Bionic investigation of a dolphin head-based hydrofoil with emphasis on energy performance and flow characteristics, Ocean Engineering 270 (2023) 113692.